The 8th European Congress on Computational Methods in Applied Sciences and Engineering
ECCOMAS Congress 2022
5-–9 June 2022, Oslo, Norway

SYMMETRY-PRESERVING DISCRETISATION METHODS FOR MAGNETOHYDRODYNAMICS

J.A. HOPMAN[1], F.X. TRIAS[1] AND J. RIGOLA[1]

[1] Heat and Mass Transfer Technological Center, Technical University of Catalonia
Carrer de Colom 11, 08222 Terrassa (Barcelona), Spain; www.cttc.upc.edu
{jannes.hopman, francesc.xavier.trias, joaquim.rigola}@upc.edu

Key words: Symmetry-preserving discretisation, Magnetohydrodynamics, OpenFOAM, Taylor-Green vortex

Abstract. In this work, the symmetry-preserving method [1, 2, 3] is extended to include magnetohydrodynamic effects, using the collocated grid arrangement of Ni *et al.* [4, 5]. The electromagnetic part is solved explicitly using the induction-less approximation and an electric potential Poisson equation. The proposed solver is implemented in OpenFOAM and tested for accuracy and stability, and compared to the method of Ni *et al.* [4, 5]. A new benchmark case using a Taylor-Green vortex in a transverse magnetic field is used, for which kinetic energy budget terms are compared to the analytical solutions. Finally, Hunt's case is used to compare flow profiles to the analytical solutions. Influence of the spatial discretisation on accuracy and stability is also examined by solving both cases on meshes with variable degrees of distortion. The symmetry-preserving method showed accuracy on Cartesian meshes and stability even on extremely distorted meshes, whereas the method of Ni *et al.* [4, 5] showed less accurate conservation of current density and was not able to produce stable solutions on the extremely distorted meshes.

1 INTRODUCTION

Magnetohydrodynamic (MHD) flows and specifically the flow of liquid metals through strong magnetic fields are of great interest in the development of nuclear fusion reactors. Two key elements in the fuel for the fusion reaction inside the reactors are deuterium and tritium, isotopes of hydrogen. While deuterium is abundantly available, tritium is not. It is, however, possible to generate, or "breed", tritium inside so-called breeding blankets, consisting of liquid metal flows through ducts inside the reactor. Lithium contained inside these blankets interacts with neutrons escaping from the fusion reaction [6]. The liquid metal flow interacts with the strong magnetic fields needed to contain the reaction plasma inside the core of the reactor, giving rise to MHD flow phenomena[7].

Theoretical work, dating back far, was able to predict these flow phenomena for very specific geometries and magnetic fields and sometimes even derive analytical solutions [8, 9, 10]. An important phenomenon of duct flows through transverse magnetic fields is the generation of a current perpendicular to both the flow direction and the direction of the magnetic field, following Faraday's law of induction. This induced current will in turn generate a force in the direction opposite to the flow, creating a characteristic high pressure drop in the center of the duct.

Depending on the conductivity of the duct walls, the direction of the current close to the walls will align with the magnetic field lines, resulting in a local drop in Lorentz force and causing high velocity jets, which lead to the characteristic M-shaped flow profiles in MHD duct flows.

Extending calculations to arbitrary geometries and magnetic fields gives rise to a number of main challenges faced in the MHD field [11, 12, 13]. First of all, the high Lorentz force that opposes the high pressure gradient gives rise to a delicate balance between forces, in which small computational errors can lead to great inaccuracies. Second of all, the extra solution variables are often solved with a second Poisson equation. Together with thin boundary layers requiring very fine meshes near the walls, this leads to high computational costs. Thirdly, discretising the problem and choosing adequate locations for the physical variables is difficult because of the different cross products between vector fields that are involved. And finally, numerical results are often difficult or impossible to verify using experimental results, due to extreme physical circumstances, such as high magnetic fields and high temperatures that are present in fusion reactors. This last point also underlines the importance of simulations, as opposed to experiments, in many cases.

To accurately balance the high pressure drop with the Lorentz force, it is of great importance to choose the right numerical discretisation of the equations that are involved. By preserving energy at all scales of motion, no artificial dissipation can disrupt this delicate balance. At the same time this warrants unconditional stability, which allows for appropriate meshes in arbitrary geometries and could allow lower computational cost by using lower-resolution boundary layers without losing stability. The symmetry-preserving method, developed by Verstappen and Veldman [1], conserves energy by mimicking the symmetries of the continuous operators in their discrete counterparts on staggered grids. By extending the symmetry-preserving method to account for MHD effects, an attempt can be made to address the aforementioned challenges.

Due to its simpler form and wide use in industrial codes, the collocated mesh formulation is often preferred over the staggered one. The symmetry-preserving method was extended to unstructured collocated meshes by Trias *et al.* [2] and later implemented in the widely used open source code OpenFoam, which uses these meshes, by Komen *et al.* [3]. Moreover, Ni *et al.* [4, 5] developed a method to discretise the MHD equations for these meshes, which is generally viewed as state-of-the-art. In this work these previous efforts will be combined to extend the symmetry-preserving method to account for MHD effects using OpenFOAM. Subsequently it will be shown that this method is accurate and unconditionally stable. To do so, a new benchmark case was developed using a Taylor-Green vortex (TGV) with a transverse magnetic field, for which the kinetic energy budget terms were monitored. Finally Hunt's case, an MHD flow through a rectangular duct, was solved while monitoring the pressure gradient and flow profile.

This work is structured as follows: In section 2 the method of Ni *et al.* [4, 5] is described and adjusted to comply with symmetry-preserving criteria, special emphasis is given to the interpolation method for the current density. Subsequently the test results for the TGV and Hunt's case are shown and discussed in sections 3. In section 4 the main conclusions are presented and the path for future work is described.

2 DISCRETISATION METHOD

MHD effects take place whenever an electric conductive fluid flows through a magnetic field, which induces a current. The interaction between this current and the magnetic field gives rise to an opposing Lorentz force. However, the induced current also generates a secondary magnetic field, altering the imposed field. A full set of the governing equation, combining the Navier-Stokes equations with the Maxwell equations, can be found in textbooks such as Müller and Bühler [14]. To simplify the equations, the assumption of induction-less flow is often made, characterised by a low magnetic Reynolds number ($Re_m \ll 1$), describing the coupling intensity between the velocity and magnetic field as:

$$Re_m = \frac{\text{Momentum advection}}{\text{Magnetic diffusivity}} = \mu\sigma u_0 L \tag{1}$$

where μ, σ and u_0 are the magnetic permeability, conductivity and velocity of the fluid, respectively, and L is the characteristic length scale of the flow. This approximation is valid for almost all liquid metal flows, especially in fusion reactor design. The resulting equations are as follows:

$$\frac{\partial \mathbf{u}}{\partial t} + (\mathbf{u}\cdot\nabla)\,\mathbf{u} = \nu\nabla^2\mathbf{u} - \nabla\,(p/\rho) + (\mathbf{J}\times\mathbf{B})\,/\rho \qquad \nabla\cdot\mathbf{u} = 0 \tag{2}$$

$$\mathbf{J} = \sigma\,(-\nabla\phi + \mathbf{u}\times\mathbf{B}) \qquad \nabla\cdot\mathbf{J} = 0 \tag{3}$$

Where equation (2) represent the momentum equation with an added Lorentz force term and the mass continuity equation. Equation (3) gives Ohm's law and the charge continuity equation. From equation (3) a Poisson equation can be derived for the electric potential, ϕ:

$$\nabla^2\phi = \nabla\cdot(\mathbf{u}\times\mathbf{B}) \tag{4}$$

The main advantages of the induction-less approximation are its lower complexity due to the scalar form of equation (4) in contrast to solving the vectorial magnetic field $\mathbf{B}$, a lessened non-linearity in the MHD coupling increasing numerical stability and a more straight-forward treatment of the boundary conditions [4, 5]. However, if the Lorentz force term of equation (2) is not properly discretised, this term can lead to inaccuracy in numerical codes, especially if inconsistent and non-conservative interpolations are used to calculate cell-centered field values. Since these problems were addressed by Ni *et al.* [4, 5] for collocated unstructured grids, the extension of the symmetry-preserving method for collocated unstructured grids in OpenFOAM [1, 2, 3] will be based on their method.

We first non-dimensionalise equation (2) using characteristic values for length, L, velocity, u_0, density, ρ_0, magnetic field, B_0, conductivity, σ_0, time, $\frac{L}{u_0}$, pressure, $\rho_0 u_0^2$ and current density, $\sigma_0 u_0 B_0$, leading to:

$$\frac{\partial \mathbf{u}}{\partial t} + \mathbf{u}\cdot\nabla\mathbf{u} = \frac{1}{Re}\nabla^2\mathbf{u} - \nabla\mathbf{p} + N(\mathbf{J}\times\mathbf{B}) \tag{5}$$

with the Reynolds number, $Re = \frac{u_0 L}{\nu}$, the Hartmann number, $Ha = LB_0\sqrt{\frac{\sigma_0}{\rho_0\nu}}$, which gives the ratio between electromagnetic force to viscous force and the interaction parameter, $N = \frac{Ha^2}{Re} = \frac{B_0^2 L\sigma_0}{u_0\rho_0}$, as the ratio between the former non-dimensional numbers.

A classical fractional step method [15, 16, 17] is used for the pressure-velocity coupling after which the electromagnetic fields are explicitly updated using equation (4), a second Poisson equation, following Ni *et al.* [4, 5]. Using the notation of Trias *et al.* [2], the extended symmetry-preserving method is given as follows:

$$\begin{aligned}\mathbf{u}_c^p &= \mathbf{u}_c^n - \Delta t \Omega^{-1} \left(C\left(\mathbf{u}_s^n\right) + D \right) \mathbf{u}_c^n \\ &\quad - \Gamma_{sc}^V G \tilde{\mathbf{p}}_c^p + N [\mathbf{J}_c^n]_\times \mathbf{B}_c^n \end{aligned} \tag{6a}$$

$$\mathbf{u}_s^p = \Gamma_{cs}^V \mathbf{u}_c^p \tag{6b}$$

$$L\tilde{\mathbf{p}}_c' = M \mathbf{u}_s^p \tag{6c}$$

$$\mathbf{u}_s^{n+1} = \mathbf{u}_s^p - G\tilde{\mathbf{p}}_c' \tag{6d}$$

$$\mathbf{u}_c^{n+1} = \mathbf{u}_c^p - \Gamma_{sc}^V G\tilde{\mathbf{p}}_c' \tag{6e}$$

$$\tilde{\mathbf{p}}_c^{n+1} = \tilde{\mathbf{p}}_c^p + \tilde{\mathbf{p}}_c' \tag{6f}$$

$$\mathbf{J}_c^p = [\mathbf{u}_c^{n+1}]_\times \mathbf{B}_c^{n+1} - \Gamma_{sc}^V G \boldsymbol{\phi}_c^p \tag{6g}$$

$$\mathbf{J}_s^p = \Gamma_{cs}^V \mathbf{J}_c^p \tag{6h}$$

$$L\boldsymbol{\phi}_c' = M \mathbf{J}_s^p \tag{6i}$$

$$\mathbf{J}_c^{n+1} = \Gamma_{sc}^V \left(\mathbf{J}_s^p - G\boldsymbol{\phi}_c' \right) \tag{6j}$$

$$\boldsymbol{\phi}_c^{n+1} = \boldsymbol{\phi}_c^p + \boldsymbol{\phi}_c' \tag{6k}$$

where $[\cdot]_\times$ indicates a skew-symmetric matrix form of a vector that results in a cross product between two vectors. Each step is summarised as follows:

(6a) Calculate the velocity predictor including a pressure predictor and the Lorentz force term
(6b) Interpolate the velocity predictor to the faces
(6c) Solve the pressure correction Poisson equation
(6d) Update the face velocities
(6e) Update the cell-centered velocities
(6f) Update the pressure field
(6g) Calculate the current density predictor including an electric potential predictor
(6h) Interpolate the electric potential predictor
(6i) Solve the electric potential correction Poisson equation
(6j) Update the cell-centered current density
(6k) Update the electric potential

Except for the Lorentz force term in step (6a), steps (6a)-(6f) are the same as in the symmetry-preserving method for hydrodynamics. Steps (6g)-(6k) explicitly update the current density and electric potential. The main ideas of the symmetry-preserving discretisation remain the same: Midpoint interpolation of the velocities in the initialisation of the convective operator, C, face-normal projected distances used in the face gradient operator, G, and conservative consistent interpolation from faces to cell centers, meeting the following criterion: $\Gamma_{sc} = \Omega^{-1} \Gamma_{cs}^T \Omega_s$, where

the total volumes in the volume weighting are conserved, i.e. $tr(\Omega) = tr(\Omega_s)$. Furthermore, a predictor value for the electric potential has been introduced, since it has been shown that this is a beneficial treatment for the pressure in the momentum predictor [2, 3]. This value can be chosen as $\mathbf{0}_c$ or $\boldsymbol{\phi}_c^n$, corresponding to the Chorin and Van Kan projection methods respectively [15, 18].

The criterion for interpolation leaves a freedom of choice for the interpolation weights in Γ_{cs}. Santos *et al.* [19] showed that a volume weighted interpolation, Γ_{cs}^V, leads to stability, even for highly distorted meshes. In this method the face volumes Ω_f are split in $\Omega_{f,-}$ and $\Omega_{f,+}$ by the face, so that:

$$\left[\Gamma_{cs}^V \mathbf{a}_c\right]_f = \frac{\Omega_{f,-}}{\Omega_f}[\mathbf{a}_c]_- \cdot \mathbf{n}_f + \frac{\Omega_{f,+}}{\Omega_f}[\mathbf{a}_c]_+ \cdot \mathbf{n}_f \tag{7}$$

These weights are illustrated in figure 1a. This results in the face-to-center interpolation given by:

$$\left[\Gamma_{sc}^V \alpha_s\right]_c = \sum_f \frac{\Omega_{f,c}}{\Omega_c}[\alpha_s]_f \mathbf{n}_f \tag{8}$$

In contrast, the interpolation introduced by Ni *et al.* [4, 5] is given by:

$$\left[\Gamma_{sc}^{Ni} \alpha_s\right]_c = \sum_f \frac{A_f\left(\mathbf{r}_f - \mathbf{r}_c\right)}{\Omega_c}[\alpha_s]_f \tag{9}$$

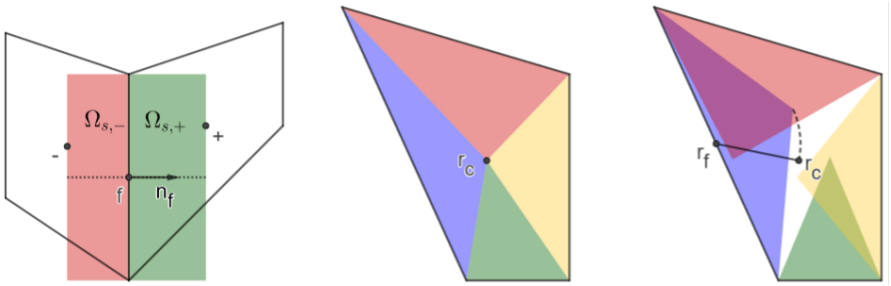

(a) (b) (c)

Figure 1: (a) Cell-to-face interpolation weights (b) Conservative face volumes (c) Non-conservative face volumes

The direction given to the scalar value of the face differs between the two methods, where equation (9) uses the direction of the vector between cell-center and face-center, $\mathbf{r}_f - \mathbf{r}_c$ as opposed to the face-normal direction, $\mathbf{n}_f$. Moreover, the interpolation from cell to face is not consistent with its opposite, i.e. $\Gamma_{sc} \neq \Omega^{-1}\Gamma_{cs}^T\Omega_s$, since a midpoint interpolation is chosen as the cell-to-face interpolator. And finally, the volume weighting of equation (9) is non-conservative, i.e. $tr(\Omega) \neq tr(\Omega_s)$, on meshes that are not circum-center, whereas the symmetry-preserving method of equation (8) does hold this criterion. This can be shown for the two-dimensional case, by drawing out triangles of half the face volumes. These triangles should sum up to the

cell volumes, as is clearly seen for the symmetry-preserving method in figure 1b. However, the height of these triangles for the method using equation (9) is given by $h = (\mathbf{r}_f - \mathbf{r}_c)\cdot\mathbf{n}_f$. In figure 1c the construction of the blue triangle is shown, together with the other resulting triangles. It can be clearly seen that the sum of these triangles does not equal the total cell volume. This gives an intuitive understanding as to why the interpolation weights are non-conservative. A similar argument holds in three dimensions, where the triangles are replaced by pyramids with a volume of one third of the face volume.
These additions to the symmetry-preserving method, including adjustments to the method of Ni *et al.* [4, 5], form a basis for a symmetry-preserving solution algorithm for MHD flows that can give accurate results and unconditional stability, even on highly distorted meshes.

3 RESULTS

This section is divided into three parts. In section 3.1, a new benchmark case is introduced, using a two-dimensional TGV inside a transverse magnetic field. Kinetic energy budget terms are calculated and compared to analytical values to compare the symmetry-preserving method to the method of Ni *et al.* [4, 5]. In section 3.2, Hunt's case is solved with both methods in order to compare the flow profiles to analytical values. This case consists of a conductive flow through a square duct inside a transverse magnetic field. Finally, the stability of both methods is discussed in section 3.3

3.1 Taylor-Green vortex

The TGV case consists of a two-dimensional square domain with $0 \leq x \leq 2\pi$, $0 \leq y \leq 2\pi$ and cyclic boundaries that contains 4 vortices [20]. The analytical solution to the field is given by the following equations:

$$u_x(x,y,t) = \sin(x)\cos(y)e^{-2\nu t} \qquad u_y(x,y,t) = -\cos(x)\sin(y)e^{-2\nu t} \tag{10}$$

$$p(x,y,t) = \frac{1}{4}(\cos(2x) + \cos(2y))e^{-4\nu t} \tag{11}$$

where non-dimensional units have been used. It can be seen from these equations that the shape of the vortices remains the same over time, the decay of their amplitude depends on the viscosity of the flow. If we introduce a transverse magnetic field in the z-direction and introduce a non-zero conductivity to the field, a current will be induced following Ohm's law. This induced current is given by:

$$\mathbf{u}\times\mathbf{B} = \begin{pmatrix} -\cos(x)\sin(y)B_z e^{-2\nu t} \\ -\sin(x)\cos(y)B_z e^{-2\nu t} \\ 0 \end{pmatrix} \tag{12}$$

We can then design an electric potential field such that the total induced current equals zero, i.e. $\nabla\phi = \mathbf{u}\times\mathbf{B}$:

$$\phi = -\sin(x)\sin(y)B_z e^{-2\nu t} \tag{13}$$

This field only has to be initialised at $t = 0$ and should develop through time, as a result of the electric potential Poisson equation. Since the induced current and Lorentz force remain zero over time, the flow should develop in the exact same way as the hydrodynamic TGV. However, when solving the equations discretely, some numerical errors may be introduced. This could lead to dissipation of kinetic energy through numerical errors, including a non-physical induced current and Lorentz force.

To monitor the accuracy of the solution, the kinetic energy budget terms were calculated and compared to their analytical values. When taking the inner product of the terms in the momentum equation (2) with velocity, the budget terms of the momentum equation are retrieved [21]:

$$
\begin{aligned}
&\partial_t E_k && \text{Evolution}\\
&= -\mathbf{u}\cdot\left(\left(\mathbf{u}\cdot\nabla\right)\mathbf{u}\right) && \text{Transport}\\
&-\mathbf{u}\cdot\left(\nabla p\right)/\rho && \text{Pressure diffusion}\\
&+\nu\nabla^2 E_k && \text{Viscous diffusion}\\
&-\nu\left(\nabla\mathbf{u}\right):\left(\nabla\mathbf{u}\right) && \text{Dissipation}\\
&+\mathbf{u}\cdot\left(\mathbf{J}\times\mathbf{B}\right)/\rho && \text{Lorentz force term}
\end{aligned}
$$

where $E_k = \frac{\mathbf{u}\cdot\mathbf{u}}{2}$. An extra budget term is retrieved for the Lorentz force term. These budget terms can be calculated locally and globally. Analytically, the only globally non-zero term is the dissipation term. Furthermore, the Lorentz force term should be locally zero everywhere.

For this particular case, $Re = 100$ and $Ha = 100$ were used. The case was run until $t = 1.0$ using a 65×65 uniform Cartesian mesh and a distorted mesh. The distortion of this mesh was achieved by displacing vertices on the mesh in x- and y-direction using a sine function. The amplitude of this function was variable, allowing for extremely distorted meshes. Two examples are given in figure 2.

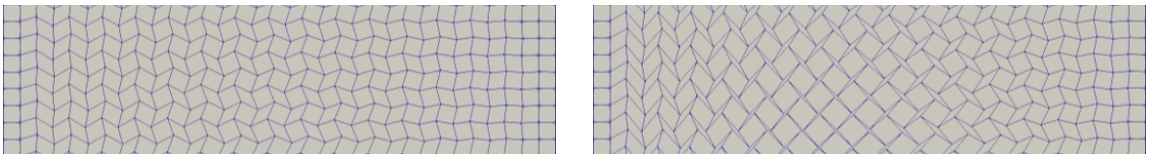

(a) Moderately distorted mesh (b) Extremely distorted mesh

Figure 2: Illustrative mesh sections

The resulting global values of the budget terms are given in figure 3, where the differences with the analytical values are plotted. It can be seen here that both solvers perform to a high degree of accuracy on the Cartesian mesh. However, when moderate mesh distortion is introduced, dissipation of kinetic energy can be seen for both methods. It seems that for both solvers, a current is generated which gives a positive value for the Lorentz force budget term. This budget term seems to be compensated by the pressure diffusion term. Finally, a decrease in the dissipation budget term is seen, which means too much energy is dissipated. It can be

seen that the effects are greater when using the method of Ni *et al.* [4, 5]. This can be the result of the improper choice for the interpolation of the current density. The interpolation of the symmetry-preserving method performs much better. However, the resulting dissipation is also non-zero. This can be due to the discretisation of the Laplacian operator in OpenFOAM, that uses a Rhie-Chow-like interpolation to avoid checkerboarding using a compact stencil. In hydrodynamic flows this only leads to a pressure error, but since the same operator is used in the electric potential Poisson equation, it can lead to an electric potential error in MHD flows [22].

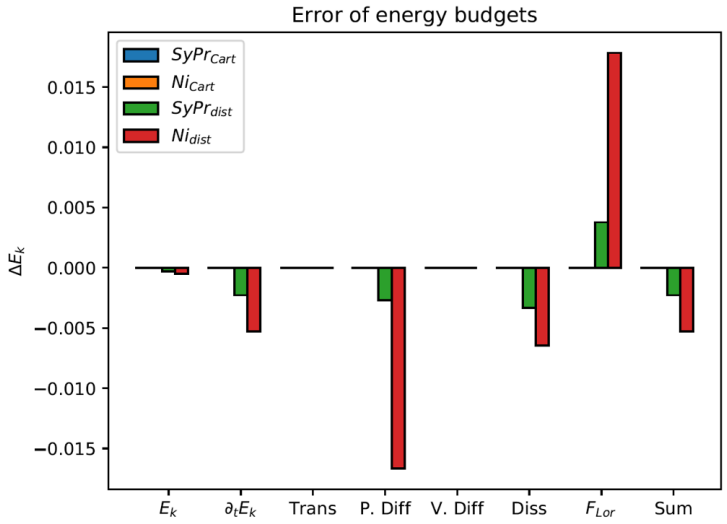

Figure 3: Difference with analytical value of the kinetic energy budget terms, on Cartesian and distorted meshes

The same data is plotted in figure 4, where a qualitative representation is given of the resulting budget terms on the moderately distorted mesh. Here it can be seen that the problems for the method of Ni *et al.* [4, 5] mainly arise in the central area of the mesh and that the problems in all budget terms coincide with the areas where the current density is non-zero. This shows the importance of the exact conservation of current density and its influence on the other kinetic energy budget terms.

3.2 Hunt's case

Hunt's case describes a laminar conductive flow through a square duct with a transverse magnetic field, perpendicular to the so-called Hartmann walls. The side walls are perfectly insulated whereas the Hartmann walls are perfectly conducting. This creates an M-shaped velocity profile with low core velocity due to a high opposing Lorentz force and velocity jets at the side walls, due to local alignment of the current density with the magnetic field lines. The solution to this case has also been calculated analytically [10] and is independent of the Reynolds number. In this case $Re = 1$ and $Ha = 30$ were used. A stretched Cartesian mesh was used so that the thin Hartmann layers contained a layer of four cells. Periodic boundaries were used in the flow direction and an average flow was maintained as $\overline{u} = 1.0$ by a variable pressure

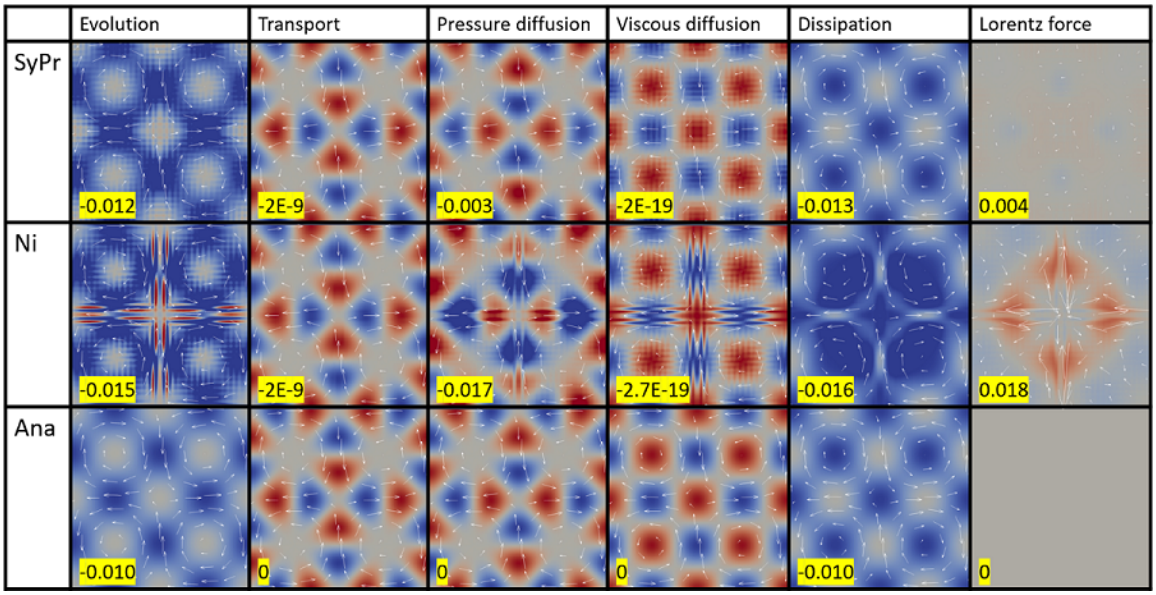

Figure 4: Qualitative comparison of the kinetic energy budget terms between the tested solvers and analytical value on the moderately distorted mesh. Global values highlighted in yellow.

gradient forcing term. A similar mesh distortion technique was used to that of the TGV case. The resulting flow profiles for the flat Hartmann layer and the jet in the side layer are shown in figure 5.

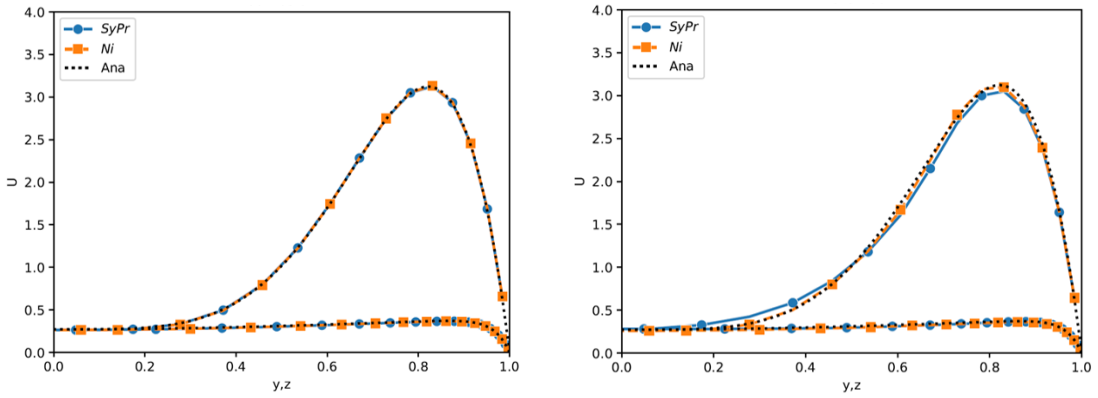

(a) Cartesian mesh

(b) Moderately distorted mesh

Figure 5: Flow profiles for Hunt's case, showing flat Hartmann profile and side profile jets

It can be seen from figure 5a that both solvers are able to accurately capture the flow profile on the Cartesian mesh. When increasing distortion the flow profiles can still be calculated to a good degree of accuracy. The method of Ni *et al.* [4, 5] shows a closer resemblance to the analytical flow profile, especially inside the jets. This does not agree with the findings of the TGV case. As can be seen from the budget terms, a compensation of errors might be the reason

behind this difference in accuracy. More calculations in different configurations should be run to confirm this.

3.3 Stability

Besides accuracy on reasonable meshes, unconditional stability is another advantage of the symmetry-preserving method. Although accuracy is not guaranteed when moving to these meshes, a non-diverging solution should always be attained. To test this, both the TGV case and Hunt's case were run with extremely distorted meshes, as illustrated in figure 2b. In both cases the method of Ni *et al.* [4, 5] was not able to calculate a proper solution, diverging quickly, whereas the symmetry-preserving method produced the results as seen in figure 6. This difference is mainly caused by the interpolation method used by each solver. Especially the cells in the centers of the quadrants, which are diamond-shaped with a high ratio between the angles, are expected to cause problems in the method of Ni *et al.* [4, 5]. This is because the conservation criterion of the face volumes, $tr(\Omega) = tr(\Omega_s)$, is most heavily violated in this type of cells, which can be visualised by increasing the skewness of the cells in figure 1.

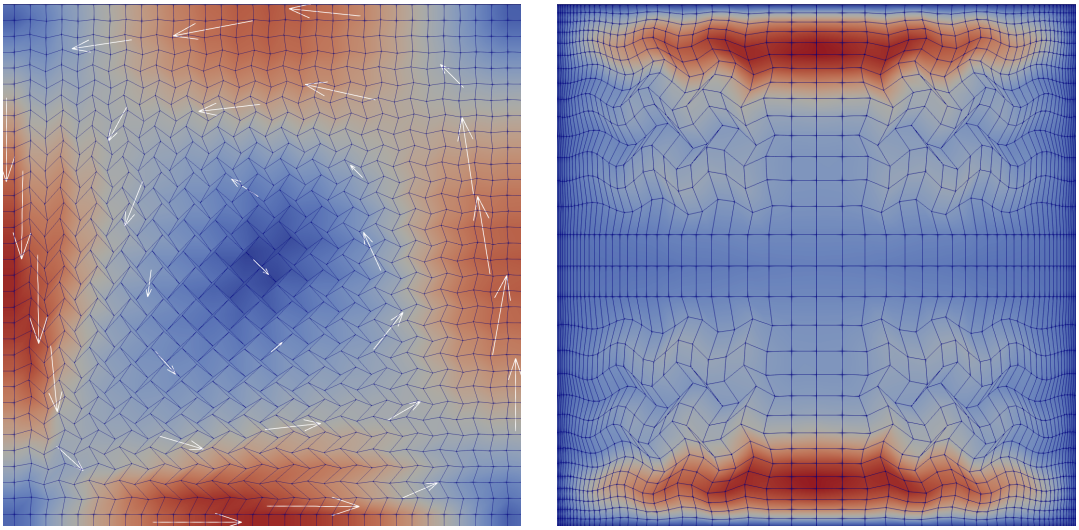

Figure 6: Stability on extremely distorted meshes using the symmetry-preserving method for TGV case (left) and Hunt's case (right)

4 CONCLUSIONS AND FUTURE WORK

The symmetry-preserving method was extended to include MHD effects and succesfully implemented into OpenFOAM. The grid arrangement of Ni *et al.* [4, 5] was used to deal with the collocated unstructured grids in OpenFOAM. The main improvements to the method of Ni *et al.* [4, 5] are the use of a symmetry-preserving interpolator and a projection method for pressure and electric potential. The new method showed improved conservation of kinetic energy budget terms on distorted meshes, mainly in the current density conservation. The new benchmark case using a TGV in a transverse magnetic field offered a useful tool to compare MHD solvers

quantitatively. Finally, unconditional stability, even on extremely distorted meshes, was shown for the symmetry-preserving method. This result was unattainable using the method of Ni *et al.* [4, 5]. To explain the slight accuracy drop of the method in Hunt's case and to further test the solver, three-dimensional turbulent cases will be run in future work.

Acknowledgements. This project is part of the RIS3CAT-FEDER, FusionCAT project (001-P-001722) of *Generalitat de Catalunya* and the RETOtwin project (PDC2021-120970-I00) of *Ministerio de Economía y Competitividad*, Spain. J.A.H. is supported by the predoctoral grant FI 2022 (2022 FI_B1 00204) of the *Catalan Agency for Management of University and Research Grants (AGAUR).*

REFERENCES

[1] R. W. Verstappen and A. E. Veldman, "Symmetry-preserving discretization of turbulent flow," *Journal of Computational Physics*, vol. 187, pp. 343–368, may 2003.

[2] F. X. Trias, O. Lehmkuhl, A. Oliva, C. D. Pérez-Segarra, and R. W. Verstappen, "Symmetry-preserving discretization of Navier-Stokes equations on collocated unstructured grids," *Journal of Computational Physics*, vol. 258, pp. 246–267, feb 2014.

[3] E. M. Komen, J. A. Hopman, E. M. Frederix, F. X. Trias, and R. W. Verstappen, "A symmetry-preserving second-order time-accurate PISO-based method," *Computers and Fluids*, vol. 225, p. 104979, jul 2021.

[4] M. J. Ni, R. Munipalli, N. B. Morley, P. Huang, and M. A. Abdou, "A current density conservative scheme for incompressible MHD flows at a low magnetic Reynolds number. Part I: On a rectangular collocated grid system," *Journal of Computational Physics*, vol. 227, no. 1, pp. 174–204, 2007.

[5] M. J. Ni, R. Munipalli, N. B. Morley, P. Huang, and M. A. Abdou, "A current density conservative scheme for incompressible MHD flows at a low magnetic Reynolds number. Part II: On an arbitrary collocated mesh," *Journal of Computational Physics*, vol. 227, no. 1, pp. 205–228, 2007.

[6] T. Hoshino, K. Kato, Y. Natori, F. Oikawa, N. Nakano, M. Nakamura, K. Sasaki, A. Suzuki, T. Terai, and K. Tatenuma, "Development of advanced tritium breeding material with added lithium for ITER-TBM," *Journal of Nuclear Materials*, vol. 417, no. 1-3, pp. 684–687, 2011.

[7] M. A. Abdou, T. A. Team, A. Ying, N. Morley, K. Gulec, S. Smolentsev, M. Kotschenreuther, S. Malang, S. Zinkle, T. Rognlien, P. Fogarty, B. Nelson, R. Nygren, K. McCarthy, M. Z. Youssef, N. Ghoniem, D. Sze, C. Wong, M. Sawan, H. Khater, R. Woolley, R. Mattas, R. Moir, S. Sharafat, J. Brooks, A. Hassanein, D. Petti, M. Tillack, M. Ulrickson, and T. Uchimoto, "On the exploration of innovative concepts for fusion chamber technology," *Fusion Engineering and Design*, vol. 54, no. 2, pp. 181–247, 2001.

[8] J. A. Shercliff, "Steady motion of conducting fluids in pipes under transverse magnetic fields," *Mathematical Proceedings of the Cambridge Philosophical Society*, vol. 49, no. 1, pp. 136–144, 1953.

[9] J. A. Shercliff, "The flow of conducting fluids in circular pipes with finite conductivity under uniform transverse magnetic fields," *Journal of Fluid Mechanics*, vol. 1, no. 6, pp. 644–666, 1956.

[10] J. Hunt, "magnetohydrodynamic flow in rectangular ducts," *Bernoulli*, vol. 21, pp. 645–658, 1964.

[11] S. Molokov and L. Bühler, "Liquid Metal Flow in a U-Bend in a Strong Uniform Magnetic Field," *Journal of Fluid Mechanics*, vol. 267, pp. 325–352, 1994.

[12] L. Bühler, "Magnetohydrodynamic flows in arbitary geometries in strong, nonuniform magnetic fields - a numerical code for the design of fusion reactor blankets," *Fusion Technology*, vol. 27, no. 1, pp. 3–24, 1995.

[13] S. Smolentsev, S. Badia, R. Bhattacharyay, L. Bühler, L. Chen, Q. Huang, H. G. Jin, D. Krasnov, D. W. Lee, E. M. De Les Valls, C. Mistrangelo, R. Munipalli, M. J. Ni, D. Pashkevich, A. Patel, G. Pulugundla, P. Satyamurthy, A. Snegirev, V. Sviridov, P. Swain, T. Zhou, and O. Zikanov, "An approach to verification and validation of MHD codes for fusion applications," *Fusion Engineering and Design*, vol. 100, pp. 65–72, 2015.

[14] U. Müller and L. Bühler, *Magnetofluiddynamics in Channels and Containers*. Springer, 2001.

[15] A. J. Chorin, "Numerical solution of the Navier-Stokes equations," *Mathematics of Computation*, vol. 22, no. 104, pp. 745–762, 1968.

[16] N. N. Yanenko, *The Method of Fractional Steps*. Springer-Verlag Berlin Heidelberg, 1971.

[17] J. Blair Perot, "An analysis of the fractional step method," *Journal of Computational Physics*, vol. 108, no. 1, pp. 51–58, 1993.

[18] J. Van Kan, "A second-order accurate pressure-correction scheme for viscous incompressible," *SIAM J. Sci. Stat. Comput.*, vol. 7, no. 3, pp. 870–891, 1986.

[19] D. Santos, J. Muela, N. Valle, and F. X. Trias, "On the interpolation problem for the poisson equation on collocated meshes," *World Congress in Computational Mechanics and ECCOMAS Congress*, vol. 600, no. January, pp. 1–12, 2021.

[20] G. I. Taylor and A. E. Green, "Mechanism of the production of small eddies from large ones," *Proceedings of the Royal Society of London. Series A - Mathematical and Physical Sciences*, vol. 158, no. 895, pp. 499–521, 1937.

[21] P. Durbin and B. Reif, *Statistical theory and modeling for turbulent flows*. Wiley& Sons, Ltd, 2 ed., 2011.

[22] C. M. Rhie and W. L. Chow, "Numerical study of the turbulent flow past an airfoil with trailing edge separation," *AIAA Journal*, vol. 21, no. 11, pp. 1525–1532, 1983.